Enzyme characterisation and kinetic modelling of the pentose phosphate pathway in yeast

Hanan L. Messiha [1,2]
Edward Kent [1,3,4]
Naglis Malys [1,2,6]
Kathleen M. Carroll [1,5]
Neil Swainston [1,4]
Pedro Mendes [1,4,7,*]
Kieran Smallbone [1,4]

[1]Manchester Centre for Integrative Systems Biology
[2]Faculty of Life Sciences
[3]Doctoral Training Centre in Integrative Systems Biology
[4]School of Computer Science
[5]School of Chemistry
University of Manchester, M13 9PL, UK.

[6]School of Life Sciences, Gibbet Hill Campus,
University of Warwick, Coventry, UK.

[7]Center for Quantitative Medicine and Department of Cell Biology,
University of Connecticut Health Center,
263 Farmington Avenue, Farmington, CT 06030, USA.

Abstract

We present the quantification and kinetic characterisation of the enzymes of the pentose phosphate pathway in *Saccharomyces cerevisiae*. The data are combined into a mathematical model that describes the dynamics of this system and allows us to predict changes in metabolite concentrations and fluxes in response to perturbations. We use the model to study the response of yeast to a glucose pulse. We then combine the model with an existing glycolysis model to study the effect of oxidative stress on carbohydrate metabolism. The combination of these two models was made possible by the standardised enzyme kinetic experiments carried out in both studies. This work demonstrates the feasibility of constructing larger network-scale models by merging smaller pathway-scale models.

*To whom correspondence should be addressed at `pedro.mendes@manchester.ac.uk`

PeerJ PrePrints | http://dx.doi.org/10.7287/peerj.preprints.146v4 | CC-BY 3.0 Open Access | received: 10 Apr 2014, published: 10 Apr 2014

Introduction

The pentose phosphate pathway (PPP) is a central and widely conserved metabolic pathway of carbohydrate metabolism which, in eukaryotic cells, is located in the cytoplasm (see Figure 1). This pathway serves two major functions: production of precursors for biosynthesis of macromolecules and production of reducing equivalents in the form of NADPH. Accordingly, these two roles are reflected in the two major phases of the PPP: in the "oxidative phase", glucose 6-phosphate (G6P) is converted into ribulose 5-phosphate (Ru5P) through the sequential action of glucose-6-phosphate dehydrogenase and 6-phosphogluconate dehydrogenase, with lactonase catalysing the hydrolysis of its 6-phosphogluconolactone (G6L) product. The "non-oxidative phase" carries out the isomerisation of Ru5P to ribose 5-phosphate (R5P), the epimerisation of Ru5P to xylulose 5-phosphate (X5P) and, through the actions of transketolase and transaldolase, a series of carbon skeleton transfers that can interconvert pentose phosphate into fructose 6-phosphate (F6P) and glyceraldehyde 3-phosphate (GAP) – both glycolytic intermediates – and erythrose 4-phosphate (E4P). The net effect of the non-oxidative phase is to produce an equilibrium between the pentoses needed for biosynthesis of macromolecules and the hexoses needed for energy management, allowing the two pools of sugars easily to interconvert. The oxidative branch is considered to be largely irreversible under normal cellular conditions, whilst the non-oxidative branch is reversible [Saggerson, 2009]. The PPP is not a simple linear pathway (see Figure 2) since several carbon atoms are recycled back into glycolysis. Furthermore, the enzyme transketolase catalyses two different reactions in the pathway, resulting in the substrates of these reactions being competitive inhibitors of one another. Thus the dynamic response of this network is hard to predict by intuition and a computational model is required for a deeper understanding.

The PPP has three main products: reduced equivalents in the form of NADPH, produced in the oxidative phase, needed in biosynthetic pathways and for maintenance of the oxidative level of cells; R5P, for the biosynthesis of all nucleic acids; and E4P, for biosynthesis of the three aromatic amino acids. Different physiological states require operation of this biochemical network in different modes: in actively growing cells, such as during culture growth in reactors, the pathway must produce a sufficient amount of all three products, since all are required in the construction of new cells. Under stress conditions growth slows and the only product in considerable demand is NADPH.

Oxidative stress causes damage to all living organisms. A number of defence and repair mechanisms have evolved that are conserved from unicellular to multicellular organisms. Cells typically respond with post-translational modification of a number of proteins, affecting both their localisation and functionality [Godon et al., 1998, Ishii et al., 2007]. In particular, oxidative stress in yeast leads to repression of glycolysis and induction of the PPP; this is crucial for maintaining the $NADPH/NADP^+$ ratio, which provides the redox power for antioxidant systems [Ralser et al., 2007].

Since the seminal work of [Glock & McLean, 1953], the pentose phosphate pathway has been subjected to a number of quantitative studies, including in yeast [Bruinenberg et al., 1983]. Mathematical models of the pathway have been created in yeast [Vaseghi et al., 1999, Ralser et al., 2007], trypanosome [Kerkhoven et al., 2013], rat [Haut et al., 1974, Sabate et al., 1995] and human [Joshi & Palsson, 1989, Mulquiney & Kuchel, 1999]. However, such studies have over-simplified, or indeed completely neglected, the non-oxidative branch of the pathway.

In this study, we aim to understand the rerouting of flux through the different modes of the PPP following in response to different cues. To that end, we kinetically quantify and characterise various enzymes in the pathway, combine these properties into a non-linear mathematical model that describes the dynamic behaviour of this system, and compare the model's predictions to experimental observations of transient metabolite concentrations following a glucose pulse. We go on to examine the response of a combined glycolysis:PPP model to oxidative stress, and compare this to measured metabolite levels.

PeerJ PrePrints | http://dx.doi.org/10.7287/peerj.preprints.146v4 | CC-BY 3.0 Open Access | received: 10 Apr 2014, published: 10 Apr 2014

Materials and Methods

Kinetics

To determine the kinetic parameters of individual enzymatic reactions of the pentose phosphate pathway, isoenzymes were purified as described previously [Malys et al., 2011]. Spectrophotometric assays were then performed for most of the isoenzymes, following a similar strategy to [Messiha et al., 2011, Smallbone et al., 2013]. Enzymes were assayed spectrophotometrically through detection of NADPH or NADH, by using coupling reactions where needed, with the exception of ribulose-5-phosphate-3-epimerase (RPE1) and ribose-5-phosphate ketol isomerase (RKI1) which where assayed using circular dichroism (CD, [Kochetov et al., 1978]). Spectrophotometric assays were coupled with enzyme(s) in which NADH or NADPH is a substrate or product so that its consumption or formation could be followed spectrophotometrically at 340 nm, using an extinction coefficient of $6.62\,\mathrm{mM}^{-1}\mathrm{cm}^{-1}$. This is unless the reaction of a particular enzyme consumes or produces NADH or NADPH, in which case no coupling enzymes were needed.

Absorbance measurements were carried out with a BMG Labtech NOVOstar plate reader (Offenburg, Germany) in 384-well format plates in a 60 μl reaction volume. All assays were performed in a standardised reaction buffer (100 mM MES, pH 6.5, 100 mM KCl, and 5 mM free magnesium in the form of $MgCl_2$) at 30 °C and were automated so that all reagents in the reaction buffer (including any coupling enzymes) are in 45 μl, the enzyme (to be assayed) in 5 μl and the substrate in 10 μl volumes as described in [Messiha et al., 2011]. For each individual enzyme, both the forward and the reverse reactions were assayed whenever possible.

Assays for each enzyme were either developed or modified from previously published methodology to be compatible with the conditions of the assay reactions (e.g. pH compatibility or unavailability of commercial substrates). The assay conditions used for each enzyme were as follows:

6-phosphogluconate dehydrogenase GND1 and GND2 were assayed in the reaction buffer in the forward reaction by direct measurement of the production of NADPH as in [He et al., 2007]. The kinetic parameters for each isoenzyme were determined by varying the concentration of each substrate (6-phosphogluconate and NADP) at fixed saturated concentration of the other.

6-phosphogluconolactonase SOL3 and SOL4 were assayed in the reaction buffer exactly according to [Schofield & Sols, 1976].

Transaldolase TAL1 and NQM1 were assayed in the reaction buffer in the forward and reverse directions according to [Tsolas & Joris, 1964, Wood, 1972]. Since sedoheptulose 7-phosphate was not available commercially, we obtained its barium salt synthesised by Chemos GmbH, and converted it to the sodium salt just prior to assay, according to [Charmantray et al., 2009].

Transketolase TKL1 and TKL2 were assayed for both of their participatory reactions in the reaction buffer in the forward and reverse directions according to [Datta & Racker, 1961, Kochetov, 1982]. The kinetic parameters were determined by varying the concentration of each substrate at a fixed saturated concentration of the other for the forward and reverse reactions.

Glucose-6-phosphate dehydrogenase ZWF1 was assayed in the reaction buffer in the forward reaction by direct measurement of the production of NADPH according to [Gould & Goheer, 1976].

Ribose-5-phosphate ketol-isomerase RKI1 was assayed for the forward and reverse reaction by CD measurements [Kochetov et al., 1978]. The assay was developed based on the fact that ribulose-5-phosphate has a maximum absorbance at 278 nm, with a measured coefficient of -2.88 $\mathrm{m°mM^{-1}mm^{-1}}$, and ribose-5-phosphate has an absorbance at 278 nm with a measured coefficient of -0.131 $\mathrm{m°mM^{-1}mm^{-1}}$. The data were collected in 400 μl in a 1 mm path length cuvette. In both directions, the change in CD angle θ at 278 nm was used to calculate the rate of reaction.

D-ribulose-5-phosphate 3-epimerase RPE1 was assayed for the forward and reverse reaction by CD measurements. The assay was developed and modified from [Karmali et al., 1983]. Ribulose-5-phosphate and xylulose-5-phosphate have an absorbance at 278 nm with a measured coefficients of -2.88 $\mathrm{m°mM^{-1}mm^{-1}}$ and +0.846 $\mathrm{m°mM^{-1}mm^{-1}}$, respectively. The change of CD θ at 278 nm was again followed to infer the rate of reaction in both directions.

All measurements are based on at least duplicate determination of the reaction rates at each substrate concentration. For each isoenzyme, the initial rates at various substrate concentrations were determined and the data obtained were analysed by the KineticsWizard [Swainston et al., 2010] and COPASI [Hoops et al., 2006] and fitted to Michaelis-Menten type kinetics (see Table 1). Whilst most of the assay methodologies performed here were reported previously, the CD measurements for ribose-5-phosphate ketol-isomerase and D-ribulose-5-phosphate 3-epimerase were newly developed for this study.

Proteomics

We attempted to measure the absolute quantities of all isoenzymes in this pathway through the QConCAT technology [Benyon et al., 2005]. Total cell protein was extracted from turbidostat yeast cultures as described earlier [Carroll et al., 2011]. Data analyses were performed using the PrideWizard software [Swainston et al., 2011] (see Table 2). Concentrations were then calculated from copy number using a typical cytoplasmic volume of 5 fl [Smallbone et al., 2013].

Model construction

From a modelling perspective, the enzyme kinetic constants and protein concentrations represent the parameters of the system, while the metabolite concentrations (Table 3) represent the variables. Combining the protein concentration data with those for the enzyme kinetic parameters allows a mathematical model to be produced for this system (Table 4) in ordinary differential equation format. Simple Michaelis-Menten kinetics are used for enzymatic reactions. The reactions consuming NADPH, E4P and R5P (sinks) are represented with mass-action kinetics (all set to an arbitraty rate constant of $k = 1\,\mathrm{s}^{-1}$). Initial concentrations of metabolites are set to the values we measured experimentally. The model considers, in the first instance, the PPP in isolation. Thus we consider three boundary metabolites to be fixed: F6P, G6P and GAP.

To consider oxidative stress, however, we expanded the model to combine it with our recently published model of glycolysis (that includes trehalose and glycerol metabolism) [Smallbone et al., 2013], where the enzymatic parameters were determined in the same condiditions as described here. This combined glycolysis:PPP model contains 34 reactions, and allows calculation of the concentration of 32 metabolites (variables). Importantly, it allows us to compare the joint response of both pathways to environmental perturbations.

Simulations and analyses were performed in the software COPASI [Hoops et al., 2006]. The models described here are available in SBML format [Hucka et al., 2003] from the BioModels database [Li et al., 2010] with identifiers BIOMD0000000502 (PPP in isolation) and BIOMD0000000503 (combined glycolysis:PPP); the models are also available from JWS online [Olivier & Snoep, 2004] at `http://jjj.mib.ac.uk/database/messiha/` where they can be inspected interactively.

Results

Experimental

Kinetic data were obtained for all PPP isoenzymes, with the exception of SOL3 and SOL4 which showed no activity after purification (see Table 1). Any missing kinetic parameters were taken from previous models [Vaseghi et al., 1999, Ralser et al., 2007], or given initial estimates using typical values (kcat = $10\,s^{-1}$, Km = 0.1 mM, [Bar-Even et al., 2011, Smallbone & Mendes, 2013]).

Only four of the isoenzymes (Gnd1, Sol3, Tal1 and Tkl1) were detected using the QConCAT proteomic approach. In the case of Gnd1/Gnd2 and Tal1/Nqm1, only the most abundant isoenzyme was detected in each case, and it is likely that the expression level the less abundant isoenzyme was not necessarily zero but at least it was below the detection limit. The remaining three undetected enzymes (Rki1, Rpe1 and Zwf1) were found in a previous study ([Ghaemmaghami et al., 2003], detailed in Table 2). Moreover, these are soluble cytoplasmic proteins, so we can assume they were likely present in the extracted protein preparations (rather than sequestered to membranes, and subsequently lost as insoluble material). There are two possible explanations for the failure to detect these proteins: poor or incomplete proteolysis (trypsin miscleavage) or unexpected post-translational modifications, either naturally occurring or inadvertently introduced during the experimental protocol.

There is a discrepancy between the TAP-tagged published data [Ghaemmaghami et al., 2003] and the QconCAT quantifications described here, with our study reporting twenty-fold higher values. We have observed higher values for QconCAT quantifications in a previous study on glycolytic enzymes [Carroll et al., 2011], compared to TAP-tagged values. In the same study we also compared the values obtained by QconCAT with other approaches; indeed the QconCAT method gave the highest values of all methods compared.

We note that the TAP-tagged values were obtained for haploid cells, whereas the current study uses diploid cells. We estimate the total cellular protein to be approximately 6 pg for diploid cells (though some studies give a higher value of 8 pg/cell [Sherman, 2002]), and 3–4 pg for haploid cells. This alone does not therefore account for the discrepancy; by this rationale one might expect the QconCAT values to be simply double. However, in our previous study [Carroll et al., 2011] we also raised the possibility of 'range compression', where abundant proteins are underestimated, due to limited linear range with TAP-tagged methodologies, and other approaches. It is also possible that different yeast strains, growth conditions, extraction methods and analytical workflows result in very different values, making convergence of data far from trivial.

Given these discrepancies, using the data from [Ghaemmaghami et al., 2003] directly to fill in any missing measurements would not be appropriate. Rather, in cases where one of two isoenzymes was not quantified (Gnd2, Nqm1), the same ratio was maintained as as in [Ghaemmaghami et al., 2003] (i.e. we use the same proportions of the two isoenzymes). For the remaining three undetected enzymes (Rki1, Rpe1, Zwf1) the value reported in that study was multiplied by twenty to provide an initial estimate.

Glucose pulse

In an earlier study [Vaseghi et al., 1999], changes in G6P concentration following a glucose pulse were found to follow the empirical function

$$\mathrm{G6P} = 0.9 + \frac{44.1\,t}{48.0 + t + 0.45\,t^2},$$

where t represents time in seconds.

We used this function as an input representing a glucose pulse, and compared the model's predicted changes in NADPH and P6G concentration with the experimental observations of [Vaseghi et al., 1999] (see Figure 3).

Whilst the present model contains many parameters that were measured under standardised conditions, a few parameters were not possible to determine experimentally and were therefore obtained from the literature. We thus employed the fitting strategy set out in [Smallbone et al., 2013]. The relative contribution of each parameter value to the quality of fit to time-course data was ranked using sensitivity analysis. If we were unable to closely match the data varying only the most important parameter, we tried using two parameters, and continued until the cycle was complete and a satisfactory fit was obtained. Parameters maintained their initial value where possible. Five parameters were varied in this way (see Table 5) to provide the match seen in Figure 3. Of these five, three were initial guesses, one (ZWF:Kg6l) was measured under other conditions, and only one ([Gnd1]) had been measured by us, but nonetheless fitted to the data.

Oxidative stress

One of the proteins that responds to oxidative stress is the glycolytic enzyme glyceraldehyde-3-phosphate dehydrogenase (TDH). In response to high oxidant levels this enzyme is inactivated and accumulates in the nucleus of the cell in several organisms and cell types [Chuang et al., 2005, Shenton & Grant, 2003]. Thus, we simulate *in silico* oxidative stress through reduction of TDH activity in the combined glycolysis:PPP model to 25% of its wild-type value, following the approach of [Ralser et al., 2007]. Cells also respond to the presence of oxidative agents through slower growth, which we translate in our model as reducing the requirement for E4P and R5P (the biomass precursors); we thus reduce the rate of consumption of these by two orders of magnitude from their reference values. The defence against the oxidant agent requires reductive power which is ultimately supplied by NADPH (e.g. through glutathione); we thus also increase the rate of NADPH consumption by two orders of magnitude. We may then compare predicted changes in metabolite concentrations to those measured in response to H_2O_2 treatment [Ralser et al., 2007], a typical oxidative stress agent [Godon et al., 1998].

The results of these simulations are presented in Table 6. They show that seven of the eight qualitative changes in metabolite concentrations are correctly predicted by the model. A difference between the experimental data and the predictions was only observed for the metabolite glycerol 3-phosphate (G3P), where the simulation predicts a small increase, but experimentally we observe a small decrease.

As the qualitative predictions reasonably matched the experimental data set, we moved on to calculate the influence of oxidative stress on carbon flux. Experimental measurements show that, in aerobic growth conditions on glucose minimal medium, PPP activity accounts for approximately 10% of the total consumption of glucose [Blank et al., 2005]. This is reasonably consistent with our simulations' prediction that the ratio of fluxes into PPP (via ZWF) and into glycolysis (via PGI) is 1:18, or 6%. Under oxidative stress conditions, our simulations predict that the ratio of fluxes into PPP and into glycolysis increases two-fold, corroborating the hypothesis that oxidative stress leads to a redirection of the carbohydrate flux [Ralser et al., 2007].

Control analysis

Metabolic control analysis (MCA) is a biochemical formalism, defining how variables, such as fluxes and concentrations, depend on network parameters. It stems from the work of [Kacser & Burns, 1973] and, independently, [Heinrich & Rapoport, 1974]. In Table 7 (a), we present the flux control coefficients for the (fitted) PPP model. These are measures of how a relative change in enzyme activity leads to a change in steady state flux through the system. For example, from the third row of the table, we predict that a 1% increase in GND levels would lead to a 0.153% decrease in RPE flux.

The table shows us that control of flux into the pathway (via ZWF) is dominated by ZWF, SOL, GND and NADPH oxidase (the latter representing all processes that oxidise NADPH). Returning to Figure 1, we see that these correspond to the first three steps of the pathway plus NADPH recycling – the oxidative phase. The table also shows the overall control of each step of the pathway, taken in COPASI [Hoops et al., 2006] to be the norm of the control coefficients. We see that little control is exerted by the RPE and TKL (R5P:S7P) steps. The three sinks have high overall control, and as such we would expect fluxes through the pathway to be highly dependent on growth rate and stress levels.

In the oxidative stress simulation the control distribution changes, as presented in Table 7 (b). The main observation from these data is that the control of the pathway input flux by the NADPH oxidase is now much lower – this is somewhat expected since the rate of this step increased 100× and thus became less limiting. Less intuitive is the reduction of overall control of the network by RKI (the reaction that produces ribose 5-phosphate, which is then used for nucleic acid biosynthesis). However this result implies that, under oxidative stress, the PPP is essentially insensitive to the "pull" from ribose use for nucleic acid synthesis, which agrees with the observation that growth is arrested under these conditions.

Discussion

The pentose phosphate pathway, depicted in Figure 1, is a central pathway in yeast and in most organisms and serves two main functions: maintenance of the NADPH:$NADP^+$ ratio, and production of several precursors for biosynthesis of macromolecules. These two roles of the pathway are mirrored in its structure and it consists of two semi-independent parts; the oxidative branch reduces $NADP^+$, whilst the non-oxidative branch creates R5P, a precursor for nucleic acid biosynthesis, or E4P, a precursor for aromatic amino acids and some vitamins. The PPP is intimately connected with glycolysis as it diverts some of its flux away from energy production. Furthermore, the two pathways have three metabolites in common: G6P, F6P and GAP.

In order to describe a biological system such as PPP quantitatively, the kinetic properties of all its components need to be established in conditions close to the physiological [van Eunen et al., 2010, Messiha et al., 2011]. Where possible, they should represent a system in steady state, where all measurements, even if carried out at different times, are performed under identical conditions. Following the methodology previously applied to glycolysis [Smallbone et al., 2013], robust and standardised enzyme kinetics and quantitative proteomics measurements were applied to the enzymes of the pentose phosphate pathway in the *S. cerevisiae* strain YDL227C. The resulting data are integrated in a kinetic model of the pathway. This is in contrast to previous studies [Vaseghi et al., 1999, Ralser et al., 2007], where kinetic parameters were taken from various literature sources and different organisms:

> "The kinetic constants were determined using enzymes from five different species (human, cow, rabbit, yeast, *E. coli*) in different laboratories over a period of more than three decades. Consequently, it cannot be expected that the simulations coincide quantitatively with the measured metabolite concentrations." [Ralser et al., 2007]

We may have more confidence in our model, whose parameters were determined under standardised conditions. We thus use the model to study the response of the pentose phosphate pathway to a glucose pulse (Figure 3). We go on to use model to study the combined response of glycolysis and PPP to oxidative stress, and find that a considerable amount of flux is rerouted through the PPP.

Our modelling approach also reveals a discrepancy between the observed change in G3P levels following stress cannot be predicted by current understanding of glycolysis and PPP; following the "cycle of knowledge" [Kell, 2006], it is of interest to direct future focus towards glycerol metabolism in order to improve the accuracy of this model.

It is important to highlight that we were not able here to quantify the concentration of all enzymes in the pathway, thus having to rely on crude estimates. The physiological conditions under which the cells were measured by [Ghaemmaghami et al., 2003] were very different than those used here, which could result in inaccurate estimates for the concentration of several enzymes. However the fact that we have measured k_{cat} values for those enzymes will allow easy correction of the model if accurate enzyme concentrations are determined later. Indeed, these data will allow to account for changes in enzyme concentrations resulting from a longer term response of the cells, through protein degradation or increased protein synthesis rate due to changes at the level of transcription and translation.

The combined PPP and glycolysis model demonstrates the value of standardised enzyme kinetic measurements – models thus parameterised can be combined to expand their scope, eventually forming large-scale models of metabolism [Snoep, 2005, Snoep et al., 2006, Smallbone & Mendes, 2013]. Indeed the combined glycolysis:PPP model could be expanded to consider enzyme concentrations as variables (through accounting for their synthesis and degradation, reflecting gene expression and signalling) which would improve its utility in predicting a broader array of conditions. Such an expansion of models to cover wider areas of metabolism and cellular biochemistry will lead to *digital organisms*, as shown in a recent proof of principle for the simple bacterium *Mycoplasma genitalium* [Karr et al., 2012].

PeerJ PrePrints | http://dx.doi.org/10.7287/peerj.preprints.146v4 | CC-BY 3.0 Open Access | received: 10 Apr 2014, published: 10 Apr 2014

The "bottom-up" strategy used here is to combine compatible kinetic models (PPP and glycolysis), expanding them towards a larger metabolic model. An alternative ("top-down") strategy is to start with a large structural yeast network [Herrgård et al., 2008, Dobson et al., 2010, Heavner et al., 2012, Heavner et al., 2013, Aung et al., 2013], then add estimated kinetic parameters and, through successive rounds of improvement, incorporate measured parameters [Smallbone et al., 2010, Smallbone & Mendes, 2013, Stanford et al., 2013], in an automated manner where possible [Li et al., 2010, Büchel et al., 2013]. Can these two strategies be combined into a more robust and scalable approach?

In summary, we present here a model of the yeast pentose phosphate pathway that we believe is the most realistic so far, including experimentally determined kinetic parameters for its enzymes and physiological enzyme concentrations. A more complex model resulting from the combination of this PPP model with a previous glycolytic model [Smallbone et al., 2013] was possible due to the standardised way in which the kinetic parameters were measured. This opens up the prospect of expanding models to eventually cover the entire metabolism of a cell in a way that makes them compatible with a further improvement, by including the effects of changes in gene expression.

Acknowledgements

PM thanks Ana M Martins for early discussions about the PPP.

References

[Aung et al., 2013] Aung HW, Henry SA, Walker LP. 2013. Revising the representation of fatty acid, glycerolipid, and glycerophospholipid metabolism in the consensus model of yeast metabolism. *Ind Biotech* 9:215–228. doi:10.1089/ind.2013.0013

[Bar-Even et al., 2011] Bar-Even A, Noor E, Savir Y, Liebermeister W, Davidi D, Tawfik DS, Milo R. 2011. The moderately efficient enzyme: evolutionary and physicochemical trends shaping enzyme parameters. *Biochemistry* 50:4402–4410. doi:10.1021/bi2002289

[Benyon et al., 2005] Beynon RJ, Doherty MK, Pratt JM, Gaskell SJ. 2005. Multiplexed absolute quantification in proteomics using artificial QCAT proteins of concatenated signature peptides. *Nature Methods* 2:587–589. doi:10.1038/nmeth774

[Blank et al., 2005] Blank LM, Kuepfer L, Sauer U. 2005. Large-scale 13C-flux analysis reveals mechanistic principles of metabolic network robustness to null mutations in yeast. *Genome Biology* 6:R49. doi:10.1186/gb-2005-6-6-r49

[Bruinenberg et al., 1983] Bruinenberg PM, Van Dijken JP, Scheffers WA. 1983. A theoretical analysis of NADPH production and consumption in yeasts. *Journal of General Microbiology* 129:953–964. doi:10.1099/00221287-129-4-953

[Büchel et al., 2013] Büchel F, Rodriguez N, Swainston N, Wrzodek C, Czauderna T, Keller R, Mittag F, Schubert M, Glont M, Golebiewski M, van Iersel M, Keating S, Rall M, Wybrow M, Hermjakob H, Hucka M, Kell DB, M?ller W, Mendes P, Zell A, Chaouiya C, Saez-Rodriguez J, Schreiber F, Laibe C, Dr?ger A, Le Novère N. 2013. Path2Models: large-scale generation of computational models from biochemical pathway maps. *BMC Systems Biology* 7:116. doi:10.1186/1752-0509-7-116

[Carroll et al., 2011] Carroll KM, Simpson DM, Eyers CE, Knight CG, Brownridge P, Dunn WB, Winder CL, Lanthaler K, Pir P, Malys N, Kell DB, Oliver SG, Gaskell SJ, Beynon RJ. 2011. Absolute quantification of the glycolytic pathway in yeast: deployment of a complete QconCAT approach. *Molecular and Cellular Proteomics* 10:M111.007633. doi:10.1074/mcp.M111.007633

[Charmantray et al., 2009] Charmantray F, Hélaine V, Legereta B, Hecquet L. 2009. Preparative scale enzymatic synthesis of D-sedoheptulose-7-phosphate from β-hydroxypyruvate and D-ribose-5-phosphate. *Journal of Molecular Catalysis B: Enzymatic* 57:6-9. doi:10.1016/j.molcatb.2008.06.005

[Chuang et al., 2005] Chuang DM, Hough C, Senatorov VV. 2005. Glyceraldehyde-3-phosphate dehydrogenase, apoptosis, and neurodegenerative diseases. *Annual Review of Pharmacology and Toxicology* 45:269–290. doi:10.1146/annurev.pharmtox.45.120403.095902

[Datta & Racker, 1961] Datta AG, Racker E. 1961. Mechanism of action of transketolase. I. Crystalization and properties of yeast enzyme. *Journal of Biological Chemistry* 236:617–623.

[Dobson et al., 2010] Dobson PD, Smallbone K, Jameson D, Simeonidis E, Lanthaler K, Pir P, Lu C, Swainston N, Dunn WB, Fisher P, Hull D, Brown M, Oshota O, Stanford NJ, Kell DB, King RD, Oliver SG, Stevens RD, Mendes P. 2010. Further developments towards a genome-scale metabolic model of yeast. *BMC Systems Biology* 4:145. doi:10.1186/1752-0509-4-145

[Ghaemmaghami et al., 2003] Ghaemmaghami S, Huh WK, Bower K, Howson RW, Belle A, Dephoure N, O'Shea EK, Weissman JS. 2003. Dynamic rerouting of the carbohydrate flux is key to counteracting oxidative stress. *Nature* 425:737–41. doi:10.1038/nature02046

[Glock & McLean, 1953] Glock GE, McLean, P. 1953. Further studies on the properties and assay of glucose 6-phosphate dehydrogenase and 6-phosphogluconate dehydrogenase of rat liver. *Biochemical Journal* 55:400–408.

[Godon et al., 1998] Godon C, Lagniel G, Lee J, Buhler JM, Kieffer S, Perrot M, Boucherie H, Toledano MB, Labarre J. 1998. The H_2O_2 stimulon in *Saccharomyces cerevisiae*. *Journal of Biological Chemistry* 273:22480–22489. doi:10.1074/jbc.273.35.22480

[Gould & Goheer, 1976] Gould BJ, Goheer MA. 1976. Kinetic mechanism from steady-state kinetics of the reaction catalysed by baker's-yeast glucose 6-phosphate dehydrogenase in solution and covalently attached to sepharose. *Biochemical Journal* 157:389–393.

[Heavner et al., 2012] Heavner BD, Smallbone K, Barker B, Mendes P, Walker LP. 2012. Yeast 5 – an expanded reconstruction of the *Saccharomyces cerevisiae* metabolic network. *BMC Systems Biology* 6:55. doi:10.1186/1752-0509-6-55

[Heavner et al., 2013] Heavner BD, Smallbone K, Price ND, Walker LP. 2013. Version 6 of the consensus yeast metabolic network refines biochemical coverage and improves model performance. *Database* 2013:bat059. doi:10.1093/database/bat059

[Herrgård et al., 2008] Herrgård MJ, Swainston N, Dobson P, Dunn WB, Arga KY, Arvas M, Blüthgen N, Borger S, Costenoble R, Heinemann M, Hucka M, Le Novére N, Li P, Liebermeister W, Mo M, Oliveira AP, Petranovic D, Pettifer S, Simeonidis E, Smallbone K, Spasić I, Weichart D, Brent R, Broomhead DS, Westerhoff HV, Kırdar B, Penttilä M, Klipp E, Palsson BØ, Sauer U, Oliver SG, Mendes P, Nielsen J, Kell DB. 2008. A consensus yeast metabolic network obtained from a community approach to systems biology. *Nature Biotechnology* 26:1155–1160. doi:10.1038/nbt1492

[Haut et al., 1974] Haut MJ, London JW, Garfinkel D. 1974. Simulation of the pentose cycle in lactating rat mammary gland. *Biochemical Journal* 138:511–524.

[He et al., 2007] He W, Wang Y, Liu W, Zhou CZ. 2007. Crystal structure of Saccharomyces cerevisiae 6-phosphogluconate dehydrogenase Gnd1. *BMC Structural Biology* 7:38. doi:10.1186/1472-6807-7-38

[Hoops et al., 2006] Hoops S, Sahle S, Gauges R, Lee C, Pahle J, Simus N, Singhal M, Xu L, Mendes P, Kummer U. 2006. COPASI: a COmplex PAthway SImulator. *Bioinformatics* 22:3067–3074. doi:10.1093/bioinformatics/btl485

[Hucka et al., 2003] Hucka M, Finney A, Sauro HM, Bolouri H, Doyle JC, Kitano H, Arkin AP, Bornstein BJ, Bray D, Cornish-Bowden A, Cuellar AA, Dronov S, Gilles ED, Ginkel M, Gor V, Goryanin II, Hedley WJ, Hodgman TC, Hofmeyr JH, Hunter PJ, Juty NS, Kasberger JL, Kremling A, Kummer U, Le Novère N, Loew LM, Lucio D, Mendes P, Minch E, Mjolsness ED, Nakayama Y, Nelson MR, Nielsen PF, Sakurada T, Schaff JC, Shapiro BE, Shimizu TS, Spence HD, Stelling J, Takahashi K, Tomita M, Wagner J, Wang J, SBML Forum. 2003. The systems biology markup language (SBML): a medium for representation and exchange of biochemical network models. *Bioinformatics* 19:524–531. doi:10.1093/bioinformatics/btg015

[Ishii et al., 2007] Ishii N, Nakahigashi K, Baba T, Robert M, Soga T, Kanai A, Hirasawa T, Naba M, Hirai K, Hoque A, Ho PY, Kakazu Y, Sugawara K, Igarashi S, Harada S, Masuda T, Sugiyama N, Togashi T, Hasegawa M, Takai Y, Yugi K, Arakawa K, Iwata N, Toya Y, Nakayama Y, Nishioka T, Shimizu K, Mori H, Tomita M. 2007. Multiple high-throughput analyses monitor the response of *E. coli* to perturbations. *Science* 316:593–597. doi:10.1126/science.1132067

[Joshi & Palsson, 1989] Joshi A, Palsson BØ. 1989. Metabolic dynamics in the human red cell. Part I–A comprehensive kinetic model. *Journal of Theoretical Biology* 141:515–528. doi:10.1016/S0022-5193(89)80233-4

[Kacser & Burns, 1973] Kacser H, Burns JA. 1973. The control of flux. *Symposia of the Society for Experimental Biology* 27:65–104.

[Heinrich & Rapoport, 1974] Heinrich R, Rapoport TA. 1974 A linear steady-state treatment of enzymatic chains. General properties, control and effector strength. *European Journal of Biochemistry* 42:89–95. doi:10.1111/j.1432-1033.1974.tb03318.x

[Karmali et al., 1983] Karmali A, Drake AF, Spencer N. 1983. Purification, properties and assay of D-ribulose 5-phosphate 3-epimerase from human erythrocytes. *Biochemical Journal* 211:617–623.

[Karr et al., 2012] Karr JR, Sanghvi JC, Macklin DN, Gutschow MV, Jacobs JM, Bolival B Jr, Assad-Garcia N, Glass JI, Covert MW. 2012. A whole-cell computational model predicts phenotype from genotype. *Cell* 150(2):389–401. doi:10.1016/j.cell.2012.05.044

[Kell, 2006] Kell DB. 2006. Metabolomics, modelling and machine learning in systems biology: towards an understanding of the languages of cells. The 2005 Theodor Bücher lecture. *FEBS J* 273:873–894. doi:10.1128/JB.185.9.2692-2699.2003

[Kerkhoven et al., 2013] Kerkhoven EJ, Achcar F, Alibu VP, Burchmore RJ, Gilbert IH, Trybiło M, Driessen NN, Gilbert D, Breitling R, Bakker BM, Barrett MP. Handling uncertainty in dynamic models: the pentose phosphate pathway in *Trypanosoma brucei*. *PLoS Computational Biology* In press. doi:10.1371/journal.pcbi.1003371

[Kochetov, 1982] Kochetov GA. 1982. Transketolase from yeast, rat liver and pig liver. *Methods in Enzymology* 90:209–223.

[Kochetov et al., 1978] Kochetov GA, Usmanov RA, Mevkh AT. 1978. A new method of determination of transketolase activity by asymmetric synthesis reaction. *Analytical Biochemistry* 88:296–301. doi:10.1016/0003-2697(78)90422-0

[Le Novère et al., 2009] Le Novère N N, Hucka M, Mi H, Moodie S, Schreiber F, Sorokin A, Demir E, Wegner K, Aladjem MI, Wimalaratne SM, Bergman FT, Gauges R, Ghazal P, Kawaji H, Li L, Matsuoka Y, Villéger A, Boyd SE, Calzone L, Courtot M, Dogrusoz U, Freeman TC, Funahashi A, Ghosh S, Jouraku A, Kim S, Kolpakov F, Luna A, Sahle S, Schmidt E, Watterson S, Wu G, Goryanin I, Kell DB, Sander C, Sauro H, Snoep JL, Kohn K, Kitano H. 2009. The Systems Biology Graphical Notation. *Nature Biotechnology* 27:735–741. doi:10.1038/nbt.1558

[Li et al., 2010] Li C, Donizelli M, Rodriguez N, Dharuri H, Endler L, Chelliah V, Li L, He E, Henry A, Stefan MI, Snoep JL, Hucka M, Le Novère N, Laibe C. 2010. BioModels Database: An enhanced, curated and annotated resource for published quantitative kinetic models. *BMC Systems Biology* 4:92. doi:10.1186/1752-0509-4-92

[Li et al., 2010] Li P, Dada JO, Jameson D, Spasic I, Swainston N, Carroll K, Dunn W, Khan F, Malys N, Messiha HL, Simeonidis E, Weichart D, Winder C, Wishart J, Broomhead DS, Goble CA, Gaskell SJ, Kell DB, Westerhoff HV, Mendes P, Paton NW. 2010. Systematic integration of experimental data and models in systems biology. *BMC Bioinformatics* 11:582. doi:10.1186/1471-2105-11-5822

[Malys et al., 2011] Malys N, Wishart JA, Oliver SG, McCarthy JEG. 2011. Protein production in *Saccharomyces cerevisiae* for systems biology studies. *Methods in Enzymology* 500:197–222. doi:10.1016/B978-0-12-385118-5.00011-6

[Messiha et al., 2011] Messiha HL, Malys N, Carroll K. 2011. Towards full quantitative description of yeast metabolism: a systematic approach for estimating the kinetic parameters of isoenzymes under in vivo like conditions. *Methods in Enzymology* 500:215–231. doi:10.1016/B978-0-12-385118-5.00012-8

[Mulquiney & Kuchel, 1999] Mulquiney PJ, Kuchel PW. 1999. Model of 2,3-bisphosphoglycerate metabolism in the human erythrocyte based on detailed enzyme kinetic equations: equations and parameter refinement. *Biochemical Journal* 342:581–596.

[Olivier & Snoep, 2004] Olivier BG, Snoep JL. 2004. Web-based kinetic modelling using JWS Online. *Bioinformatics* 20:2143–2144. doi:10.1093/bioinformatics/bth200

[Ralser et al., 2007] Ralser M, Wamelink MM, Kowald A, Gerisch B, Heeren G, Struys EA, Klipp E, Jakobs C, Breitenbach M, Lehrach H, Krobitsch S. 2007. Dynamic rerouting of the carbohydrate flux is key to counteracting oxidative stress. *Journal of Biology* 6:10. doi:10.1186/jbiol61

[Sabate et al., 1995] Sabate L, Franco R, Canela EI, Centelles JJ, Cascante M. 1995. A model of the pentose phosphate pathway in rat liver cells. *Molecular and Cellular Biochemistry* 142:9–17. doi:10.1007/BF00928908

[Saggerson, 2009] Saggerson D. 2009. Getting to grips with the pentose phosphate pathway in 1953. *Biochemical Journal*. doi:10.1042/BJ20081961

[Schofield & Sols, 1976] Schofield PJ, Sols A. 1976. Rat liver 6-phosphogluconolactonase: a low Km enzyme. *Biochemical and Biophysical Research Communications* 71:1313–1318. doi:10.1016/0006-291X(76)90798-1

[Sha et al., 2013] Sha W, Martins AM, Laubenbacher R, Mendes P, Shulaev V. 2013. The genome-wide early temporal response of *Saccharomyces cerevisiae* to oxidative stress induced by cumene hydroperoxide. *PLoS ONE* 8:e74939. doi:10.1371/journal.pone.0074939

[Shenton & Grant, 2003] Shenton D, Grant CM. 2003. Protein S-thiolation targets glycolysis and protein synthesis in response to oxidative stress in the yeast *Saccharomyces cerevisiae*. *Biochemical Journal* 1:513–519. doi:10.1042/BJ20030414

[Sherman, 2002] Sherman F. 2002. Getting started with yeast. *Methods in Enzymology* 350:3–41.

[Smallbone et al., 2010] Smallbone K, Simeonidis E, Swainston N, Mendes P. 2010. Towards a genome-scale kinetic model of cellular metabolism. *BMC Systems Biology* 4:6. doi:10.1186/1752-0509-4-6

[Smallbone et al., 2013] Smallbone K, Messiha HL, Carroll KM, Winder CL, Malys N, Dunn WB, Murabito E, Swainston N, Dada JO, Khan F, Pir P, Simeonidis E, Spasić I, Wishart J, Weichart D, Hayes NW, Jameson D, Broomhead DS, Oliver SG, Gaskell SJ, McCarthy JE, Paton NW, Westerhoff HV, Kell DB, Mendes P. 2013. A model of yeast glycolysis based on a consistent kinetic characterisation of all its enzymes. *FEBS Letters* 587:2832–2841. doi:10.1016/j.febslet.2013.06.043

[Smallbone & Mendes, 2013] Smallbone K, Mendes P. 2013. Large-scale metabolic models: from reconstruction to differential equations. *Industrial Biotechnology* 9:179–184. doi:10.1089/ind.2013.0003

[Snoep, 2005] Snoep JL. 2005. The Silicon Cell initiative: working towards a detailed kinetic description at the cellular level. *Current Opinion in Biotechnology* 16:336–343. doi:10.1016/j.copbio.2005.05.003

[Snoep et al., 2006] Snoep JL, Bruggeman F, Olivier BG, Westerhoff HV. 2006. Towards building the silicon cell: a modular approach. *Biosystems* 83:207–216. doi:10.1016/j.biosystems.2005.07.006

[Stanford et al., 2013] Stanford NJ, Lubitz T, Smallbone K, Klipp E, Mendes P, Liebermeister W. 2013. Systematic construction of kinetic models from genome-scale metabolic networks. *PLoS ONE* 8:e79195. doi:10.1371/journal.pone.0079195

[Swainston et al., 2010] Swainston N, Golebiewski M, Messiha HL, Malys N, Kania R, Kengne S, Krebs O, Mir S, Sauer-Danzwith H, Smallbone K, Weidemann A, Wittig U, Kell DB, Mendes P, Müller W, Paton NW, Rojas I. 2010. Enzyme kinetics informatics: from instrument to browser. *FEBS Journal* 277:3769–3779. doi:10.1111/j.1742-4658.2010.07778.x

[Swainston et al., 2011] Swainston N, Jameson D, Carroll K. 2011. A QconCAT informatics pipeline for the analysis, visualization and sharing of absolute quantitative proteomics data. *Proteomics* 11:329–333. doi:10.1002/pmic.201000454

[Tsolas & Joris, 1964] Tsolas O and Joris L. 1964. Transaldolase In: Boyer PD, ed. The Enzymes 7. New York: Academic Press, 259?-280.

[van Eunen et al., 2010] van Eunen K, Bouwman J, Daran-Lapujade P, Postmus J, Canelas AB, Mensonides FI, Orij R, Tuzun I, van den Brink J, Smits GJ, van Gulik WM, Brul S, Heijnen JJ, de Winde JH, Teixeira de Mattos MJ, Kettner C, Nielsen J, Westerhoff HV, Bakker BM. 2010. Measuring enzyme activities under standardized *in vivo*-like conditions for systems biology. *FEBS Journal* 277:749–760. doi:10.1111/j.1742-4658.2009.07524.x

[Vaseghi et al., 1999] Vaseghi S, Baumeister A, Rizzi M, Reuss M. 1999. In vivo dynamics of the pentose phosphate pathway in *Saccharomyces cerevisiae*. *Metabolic Engineering* 1:128–140. doi:10.1006/mben.1998.0110

[Wood, 1972] Wood T. 1972. The forward and reverse reactions of transaldolase. *FEBS Letters,* 52:153-155. doi:10.1016/0014-5793(72)80474-5

Figure 1: Pictorial representation of the pentose phosphate pathway in Systems Biology Graphical Notation format (SBGN, [Le Novère et al., 2009])), where a circle represents a simple chemical, a rounded rectangle represents a macromolecule, the empty set symbol represents a sink, and a box represents a process.

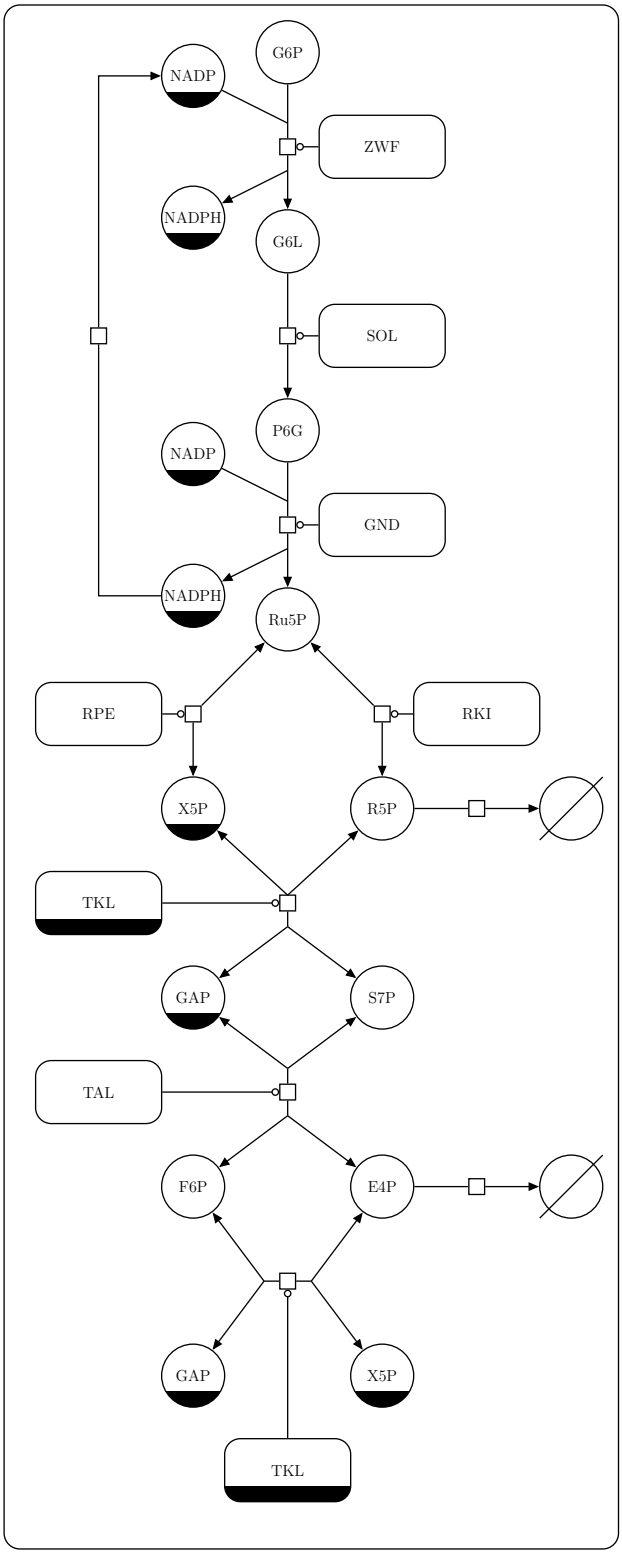

Figure 2: Pictorial representation of the combined glycolysis:PPP model in SBGN format. Note that the enzymes are ommited from this diagram for clarity of the layout.

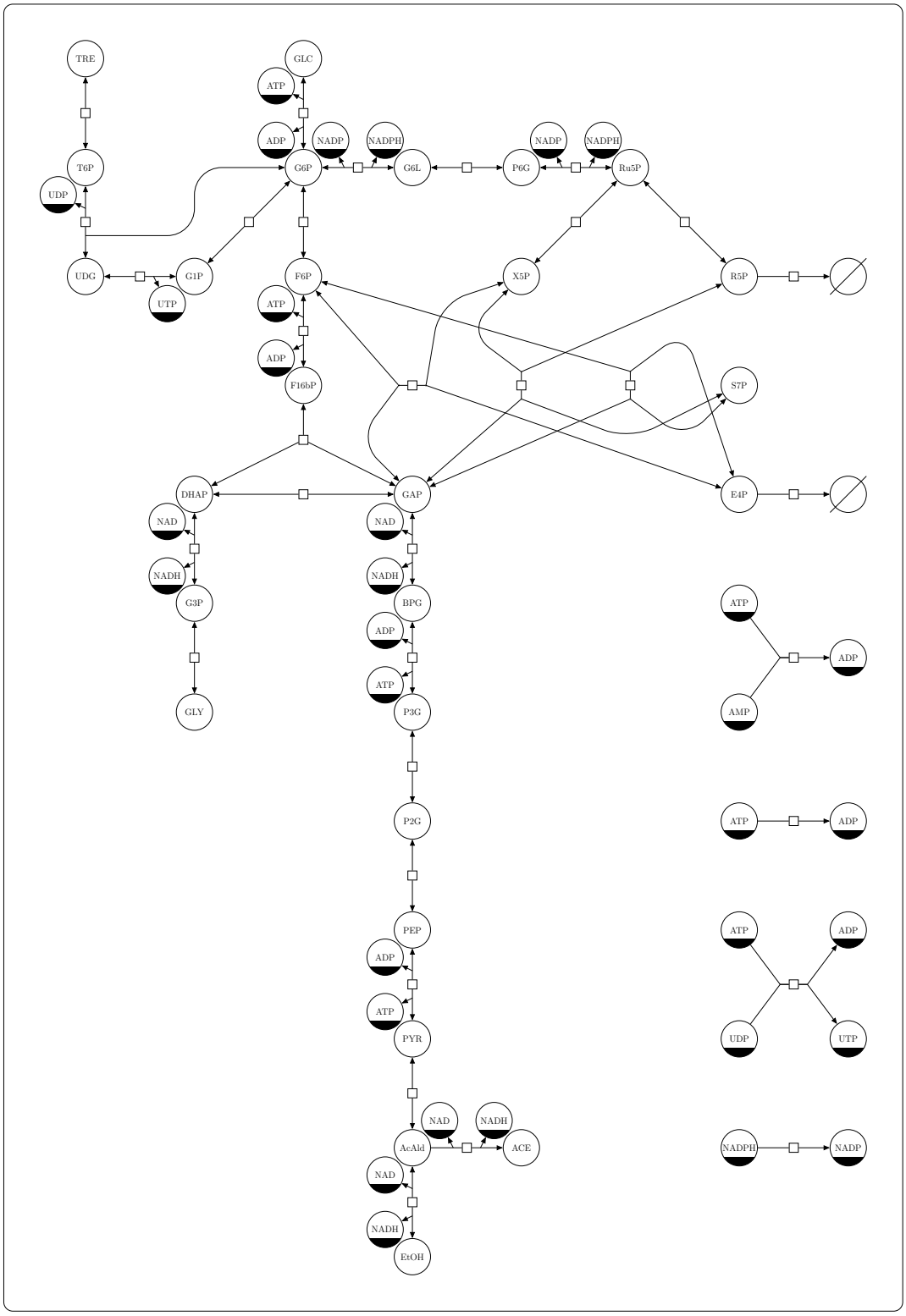

Figure 3: A pulse in G6P is applied to the model and a comparison is made between the predicted (lines) and experimentally-determined (circles) concentrations of NADPH and P6G. The system is first run to steady state before application of the pulse.

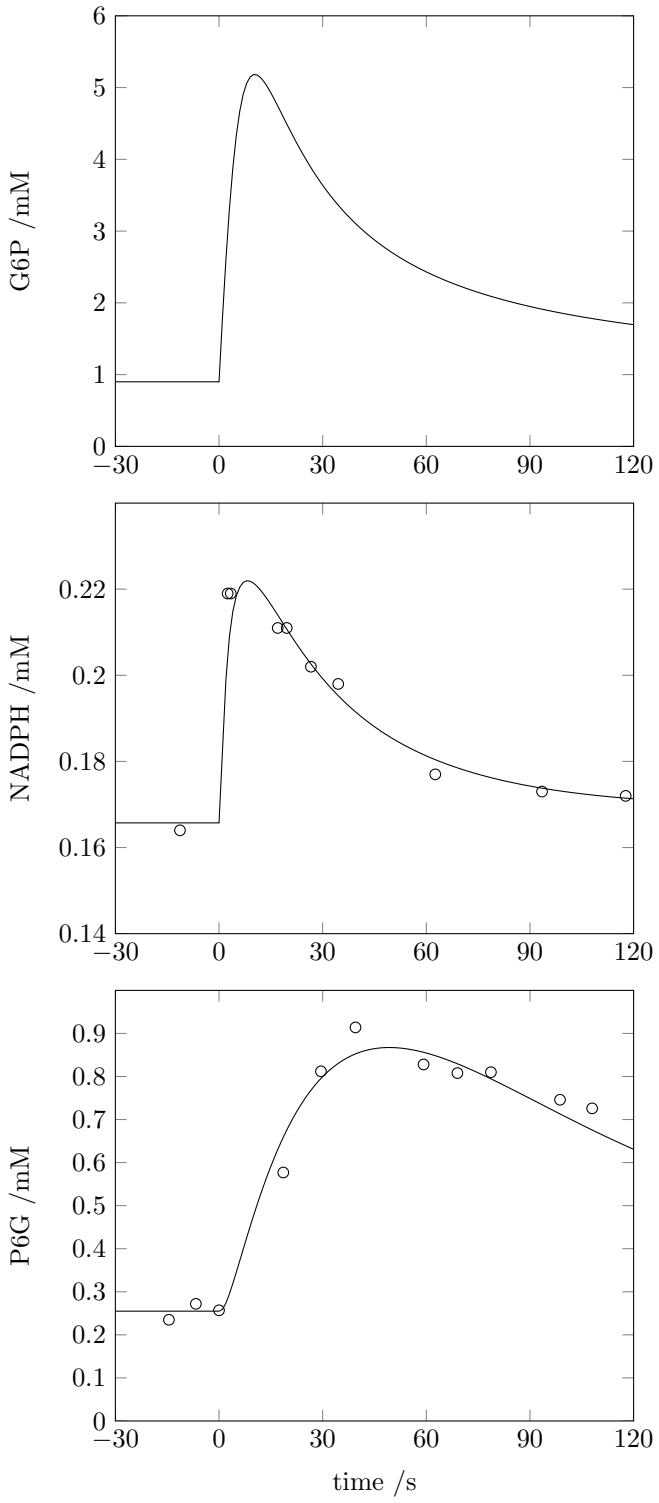

Table 1: Enzyme kinetic parameters used in the model. Standard errors are given where the parameters were measured in this study.

reaction	isoenzyme	parameter	value	units	SEM / reference
GND	Gnd1	kcat	28.0	s^{-1}	±1.8%
GND	Gnd1	Kp6g	0.062	mM	±7.7%
GND	Gnd1	Knadp	0.094	mM	±14%
GND	Gnd1	Kru5p	0.1	mM	–
GND	Gnd1	Knadph	0.055	mM	[Vaseghi et al., 1999]
GND	Gnd2	kcat	27.3	s^{-1}	±2.5%
GND	Gnd2	Kp6g	0.115	mM	±12%
GND	Gnd2	Knadp	0.094	mM	±8.9%
GND	Gnd2	Kru5p	0.1	mM	–
GND	Gnd2	Knadph	0.055	mM	[Vaseghi et al., 1999]
RKI	Rki1	kcat	335	s^{-1}	±9.5%
RKI	Rki1	Kru5p	2.47	mM	±53%
RKI	Rki1	Kr5p	5.70	mM	±19%
RKI		Keq	4.0	1	[Vaseghi et al., 1999]
RPE	Rpe1	kcat	4020	s^{-1}	±0.097%
RPE	Rpe1	Kr5up	5.97	mM	±0.50%
RPE	Rpe1	Kx5p	7.70	mM	±0.30%
RPE		Keq	1.4	1	[Vaseghi et al., 1999]
SOL	Sol3	kcat	10	s^{-1}	–
SOL	Sol3	Kg6l	0.8	mM	[Ralser et al., 2007]
SOL	Sol3	Kp6g	0.1	mM	–
TAL	Tal1	kcat	0.694	s^{-1}	±2.8%
TAL	Tal1	Kgap	0.272	mM	±12%
TAL	Tal1	Ks7p	0.786	mM	±9.7%
TAL	Tal1	Kf6p	1.44	mM	±15%
TAL	Tal1	Ke4p	0.362	mM	±15%
TAL	Nqm1	kcat	0.694	s^{-1}	–
TAL	Nqm1	Kgap	0.272	mM	–
TAL	Nqm1	Ks7p	0.786	mM	–
TAL	Nqm1	Kf6p	1.04	mM	±25%
TAL	Nqm1	Ke4p	0.305	mM	±8.0%
TAL		Keq	1.05	1	[Vaseghi et al., 1999]
TKL	Tkl1	kcat (E4P:F6P)	47.1	s^{-1}	±2.9%
TKL	Tkl1	kcat (R5P:S7P)	40.5	s^{-1}	±2.9%
TKL	Tkl1	Kx5p	0.67	mM	±13%
TKL	Tkl1	Ke4p	0.946	mM	±8.7%
TKL	Tkl1	Kr5p	0.235	mM	±13%
TKL	Tkl1	Kgap	0.1	mM	[Ralser et al., 2007]
TKL	Tkl1	Kf6p	1.1	mM	[Ralser et al., 2007]
TKL	Tkl1	Ks7p	0.15	mM	[Ralser et al., 2007]
TKL		Keq (E4P:F6P)	10.0	1	[Vaseghi et al., 1999]
TKL		Keq (R5P:S7P)	1.2	1	[Vaseghi et al., 1999]

PeerJ PrePrints | http://dx.doi.org/10.7287/peerj.preprints.146v4 | CC-BY 3.0 Open Access | received: 10 Apr 2014, published: 10 Apr 2014

ZWF	Zwf1	kcat	189	s^{-1}	±1.2%
ZWF	Zwf1	Kg6p	0.042	mM	±5.0%
ZWF	Zwf1	Knadp	0.045	mM	±6.3%
ZWF	Zwf1	Kg6l	0.1	mM	–
ZWF	Zwf1	Knadph	0.017	mM	[Ralser et al., 2007]
NADPH oxidase		k	1	s^{-1}	–
E4P sink		k	1	s^{-1}	–
R5P sink		k	1	s^{-1}	–

PeerJ PrePrints | http://dx.doi.org/10.7287/peerj.preprints.146v4 | CC-BY 3.0 Open Access | received: 10 Apr 2014, published: 10 Apr 2014

Table 2: Protein levels used in the model. Standard errors are given where measured in this study.

reaction	isoenzyme	UniProt	#/cell	SEM	[Ghaemmaghami et al., 2003]	mM
GND	Gnd1	P38720	1,010,000	±21%	101,000	0.335
GND	Gnd2	P53319			556	0.003
RKI	Rki1	Q12189			5,680	0.05
RPE	Rpe1	P46969			3,310	0.03
SOL	Sol3	P38858	89,000	±27%	3,420	0.0296
TAL	Tal1	P15019	434,000	±10%	53,000	0.144
TAL	Nqm1	P53228			1,920	0.02
TKL	Tkl1	P23254	1,370,000	±36%	40,300	0.455
ZWF	Zwf1	P11412			15,000	0.1

PeerJ PrePrints | http://dx.doi.org/10.7287/peerj.preprints.146v4 | CC-BY 3.0 Open Access | received: 10 Apr 2014, published: 10 Apr 2014

Table 3: Initial metabolite concentrations used in the model, and a comparison to their steady state levels. G6P, F6P and GAP are boundary metabolites. Note that NADP and NADPH form a conserved moeity with (experimentally-determined) constant total concentration 0.33 mM.

metabolite	ChEBI id	concentration (mM) initial	concentration (mM) steady state	reference
E4P	16897	0.029	0.0130	[Vaseghi et al., 1999]
G6L	57955	0.1	2.25	–
NADP	58349	0.17	0.166	[Vaseghi et al., 1999]
NADPH	57783	0.16	0.164	[Vaseghi et al., 1999]
P6G	58759	0.25	0.255	[Vaseghi et al., 1999]
R5P	18189	0.118	0.0940	[Vaseghi et al., 1999]
Ru5P	58121	0.033	0.0379	[Vaseghi et al., 1999]
S7P	57483	0.082	0.0902	[Vaseghi et al., 1999]
X5P	57737	0.041	0.0539	[Vaseghi et al., 1999]
G6P	16897	0.9		[Vaseghi et al., 1999]
F6P	57579	0.325		[Smallbone et al., 2013]
GAP	58027	0.067		[Smallbone et al., 2013]

PeerJ PrePrints | http://dx.doi.org/10.7287/peerj.preprints.146v4 | CC-BY 3.0 Open Access | received: 10 Apr 2014, published: 10 Apr 2014

Table 4: Kinetic rate laws for the reaction velocities used in the model.

enzyme	E.C.	reaction	rate law
GND	1.1.1.44	$\mathrm{P6G} + \mathrm{NADP} \longrightarrow \mathrm{Ru5P} + \mathrm{NADPH}$	$\frac{\mathrm{Gnd\,kcat}}{\mathrm{Kp6g\,Knadp}} \frac{\mathrm{P6G\,NADP}}{(1 + \mathrm{P6G/Kp6g} + \mathrm{Ru5P/Kru5p})\,(1 + \mathrm{NADP/Knadp} + \mathrm{NADPH/Knadph})}$
RKI	5.3.1.6	$\mathrm{Ru5P} \longleftrightarrow \mathrm{R5P}$	$\frac{\mathrm{Rki1\,kcat}}{\mathrm{Kru5p}} \frac{\mathrm{Ru5P} - \mathrm{R5P/Keq}}{1 + \mathrm{Ru5P/Kru5p} + \mathrm{R5P/Kr5p}}$
RPE	5.1.3.1	$\mathrm{Ru5P} \longleftrightarrow \mathrm{X5P}$	$\frac{\mathrm{Rpe1\,kcat}}{\mathrm{Kru5p}} \frac{\mathrm{Ru5P} - \mathrm{X5P/Keq}}{1 + \mathrm{Ru5P/Kru5p} + \mathrm{X5P/Kx5p}}$
SOL	3.1.1.31	$\mathrm{G6L} \longrightarrow \mathrm{P6G}$	$\frac{\mathrm{Sol3\,kcat}}{\mathrm{Kg6l}} \frac{\mathrm{G6L}}{1 + \mathrm{G6L/Kg6l} + \mathrm{P6G/Kp6g}}$
TAL	2.2.1.2	$\mathrm{GAP} + \mathrm{S7P} \longleftrightarrow \mathrm{F6P} + \mathrm{E4P}$	$\frac{\mathrm{Tal\,kcat}}{\mathrm{Kgap\,Ks7p}} \frac{\mathrm{GAP\,S7P} - \mathrm{F6P\,E4P/Keq}}{(1 + \mathrm{GAP/Kgap} + \mathrm{F6P/Kf6p})\,(1 + \mathrm{S7P/Ks7p} + \mathrm{E4P/Ke4p})}$
TKL (E4P:F6P)	2.2.1.1	$\mathrm{X5P} + \mathrm{E4P} \longleftrightarrow \mathrm{GAP} + \mathrm{F6P}$	$\frac{\mathrm{Tkl1\,kcat}}{\mathrm{Kx5p\,Ke4p}} \frac{\mathrm{X5P\,E4P} - \mathrm{GAP\,F6P/Keq}}{(1 + \mathrm{X5P/Kx5p} + \mathrm{GAP/Kgap})\,(1 + \mathrm{E4P/Ke4p} + \mathrm{F6P/Kf6p} + \mathrm{R5P/Kr5p} + \mathrm{S7P/Ks7p})}$
TKL (R5P:S7P)	2.2.1.1	$\mathrm{X5P} + \mathrm{R5P} \longleftrightarrow \mathrm{GAP} + \mathrm{S7P}$	$\frac{\mathrm{Tkl1\,kcat}}{\mathrm{Kx5p\,Kr5p}} \frac{\mathrm{X5P\,R5P} - \mathrm{GAP\,S7P/Keq}}{(1 + \mathrm{X5P/Kx5p} + \mathrm{GAP/Kgap})\,(1 + \mathrm{E4P/Ke4p} + \mathrm{F6P/Kf6p} + \mathrm{R5P/Kr5p} + \mathrm{S7P/Ks7p})}$
ZWF	1.1.1.49	$\mathrm{G6P} + \mathrm{NADP} \longrightarrow \mathrm{G6L} + \mathrm{NADPH}$	$\frac{\mathrm{Zwf1\,kcat}}{\mathrm{Kg6p\,Knadp}} \frac{\mathrm{G6P\,NADP}}{(1 + \mathrm{G6P/Kg6p} + \mathrm{G6L/Kg6l})\,(1 + \mathrm{NADP/Knadp} + \mathrm{NADPH/Knadph})}$
NADPH oxidase		$\mathrm{NADPH} \longrightarrow \mathrm{NADP}$	$\mathrm{k} \cdot \mathrm{NADPH}$
E4P sink		$\mathrm{E4P} \longrightarrow$	$\mathrm{k} \cdot \mathrm{E4P}$
R5P sink		$\mathrm{R5P} \longrightarrow$	$\mathrm{k} \cdot \mathrm{R5P}$

PeerJ PrePrints | http://dx.doi.org/10.7287/peerj.preprints.146v4 | CC-BY 3.0 Open Access | received: 10 Apr 2014, published: 10 Apr 2014

Table 5: Parameter changes in the fitted version of the model.

reaction	parameter	initial	fitted
GND	[Gnd1]	0.335	0.013
SOL	kcat	10	4.3
SOL	Kp6g	0.1	0.5
ZWF	[Zwf1]	0.1	0.02
ZWF	Kg6l	0.1	0.01

PeerJ PrePrints | http://dx.doi.org/10.7287/peerj.preprints.146v4 | CC-BY 3.0 Open Access | received: 10 Apr 2014, published: 10 Apr 2014

Table 6: Change in experimentally-determined metabolite concentrations with and without oxidative stress and the predictions from the combined glycolysis:PPP model. Changes are presented as $\log_{10}$ ([stressed]/[reference]).

metabolite	ChEBI id	*in vivo* change	*in silico* change
DHAP	16108	0.172	0.158
F6P+G6P	47877	0.183	0.238
G3P	15978	−0.073	0.096
GAP	29052	0.176	0.173
P6G	58759	0.699	0.603
R5P	18189	0.295	1.919
Ru5P+X5P	24976	0.908	1.723
S7P	57483	1.405	3.429

PeerJ PrePrints | http://dx.doi.org/10.7287/peerj.preprints.146v4 | CC-BY 3.0 Open Access | received: 10 Apr 2014, published: 10 Apr 2014

Table 7: Flux control coefficients in the PPP model in (a) the reference state and (b) following oxidative stress. The rows represent the fluxes under control, and the columns represent the controlling reactions. The overall control values are defined by the L_2-norm of the column values.

		GND	RKI	RPE	SOL	TAL	TKL (E4P:F6P)	TKL (R5P:S7P)	ZWF	NADPH oxidase	E4P sink	R5P sink
(a)	GND	0.156	0.004	0.000	0.333	0.000	−0.001	0.000	0.128	0.374	0.000	0.005
	RKI	0.118	0.034	0.001	0.251	−0.006	0.084	0.000	0.096	0.283	0.028	0.111
	RPE	−0.153	0.251	0.010	−0.327	−0.050	0.682	−0.001	−0.125	−0.367	0.227	0.853
	SOL	0.156	0.004	0.000	0.333	0.000	−0.001	0.000	0.128	0.374	0.000	0.005
	TAL	0.772	−1.076	−0.045	1.645	0.849	−0.585	0.011	0.631	1.848	1.432	−4.483
	TKL E4P:F6P	−0.106	0.183	0.008	−0.226	−0.004	0.618	−0.001	−0.087	−0.254	0.288	0.580
	TKL R5P:S7P	0.772	−1.076	−0.045	1.645	0.849	−0.585	0.011	0.631	1.848	1.432	−4.483
	ZWF	0.156	0.004	0.000	0.333	0.000	−0.001	0.000	0.128	0.374	0.000	0.005
	NADPH oxidase	0.156	0.004	0.000	0.333	0.000	−0.001	0.000	0.128	0.374	0.000	0.005
	E4P sink	−0.063	0.122	0.005	−0.135	0.038	0.559	0.000	−0.052	−0.151	0.344	0.334
	R5P sink	0.114	0.042	0.002	0.242	−0.012	0.088	0.000	0.093	0.272	0.018	0.141
	overall	1.163	1.559	0.065	2.481	1.203	1.364	0.016	0.952	2.788	2.087	6.434
(b)	GND	0.103	0.001	0.000	0.638	0.055	0.006	0.000	0.131	0.003	−0.005	0.067
	RKI	0.159	0.001	0.000	0.984	−0.359	−0.066	0.004	0.202	0.005	0.055	0.016
	RPE	−0.044	0.001	0.000	−0.271	1.145	0.198	−0.012	−0.056	−0.001	−0.161	0.202
	SOL	0.103	0.001	0.000	0.638	0.055	0.006	0.000	0.131	0.003	−0.005	0.067
	TAL	0.009	0.000	0.000	0.055	0.934	0.013	0.002	0.011	0.000	0.017	−0.041
	TKL E4P:F6P	−0.141	0.003	0.000	−0.875	1.535	0.540	−0.038	−0.180	−0.004	−0.492	0.653
	TKL R5P:S7P	0.009	0.000	0.000	0.055	0.934	0.013	0.002	0.011	0.000	0.017	−0.041
	ZWF	0.103	0.001	0.000	0.638	0.055	0.006	0.000	0.131	0.003	−0.005	0.067
	NADPH oxidase	0.103	0.001	0.000	0.638	0.055	0.006	0.000	0.131	0.003	−0.005	0.067
	E4P sink	0.185	−0.005	0.001	1.144	0.231	−0.605	0.049	0.235	0.005	0.613	−0.852
	R5P sink	0.208	0.002	0.000	1.288	−0.784	−0.092	0.005	0.265	0.006	0.067	0.034
	overall	0.409	0.007	0.001	2.531	2.494	0.843	0.064	0.521	0.012	0.807	1.103

PeerJ PrePrints | http://dx.doi.org/10.7287/peerj.preprints.146v4 | CC-BY 3.0 Open Access | received: 10 Apr 2014, published: 10 Apr 2014

Figure 4: Saturation curves for the assays performed in this study. The original data are available from `http://dbkgroup.org:8080/mcisb-web/MeMo-RK/`